

Experimental Evidence of Surface-Plasmon Coupling in Anisotropic Hollow Nanoparticles

M. Kociak,¹ O. Stéphan,¹ L. Henrard,² V. Charbois,¹ A. Rothschild,³ R. Tenne,³ and C. Colliex^{1,4}

¹Laboratoire de Physique des Solides, Associé au CNRS, Bâtiment 510, Université Paris-Sud, 91405, Orsay, France

²Laboratoire de Physique du Solide, Facultés Universitaires Notre-Dame de la Paix, 61 rue de Bruxelles, 5000 Namur, Belgium

³Weizmann Institute, Rehovot 76100, Israel

⁴Laboratoire Aimé Cotton, Bâtiment 505, Université Paris-Sud, 91405 Orsay-Cedex, France

(Received 2 March 2001; published 26 July 2001)

We report on the investigation of surface-plasmon excitation of anisotropic WS_2 hollow nanoparticles in a near-field geometry by means of a scanning transmission electron microscope. The shell thickness influence on the electron-energy-loss-spectroscopy spectra is experimentally observed and is analyzed within a classical dielectric formalism. As for the isotropic case, we evidence one symmetric (tangential) and one antisymmetric (radial) mode. We point out the intriguing fact that, for the anisotropic case, one can relate these modes to the interband transition of the in-plane component of the dielectric tensor and to the bulk-plasmon energy of the out-of-plane component.

DOI: 10.1103/PhysRevLett.87.075501

PACS numbers: 61.46.+w, 68.37.Ef, 78.67.Ch

As the size of artificial or natural nanostructures decreases, it is important to understand their intrinsic properties compared to bulk ones. It is particularly the case for their optical and dielectric properties, i.e., the response of the valence electrons of the nanostructure to a given applied electromagnetic field. This has been clearly emphasized in recent experiments involving photon beams, both in far-field [1] and near-field [2–4] geometries, as well as in electron spectroscopy on thin films [5] and nanospheres [6].

The electromagnetic response of such nanoparticles is described by their polarizability, which is defined as the proportionality coefficient connecting the external applied potential to the induced one. The surface-plasmon excitations that are the main concern of this Letter are described in terms of resonances in the polarizability. Hereafter, we deal with the classical dielectric model for which the polarizability is obtained from the bulk dielectric tensor $\bar{\epsilon}(\omega)$. For isotropic materials, the common interpretation scheme of the ω dependence of the bulk dielectric function $\epsilon(\omega)$ is that the maxima of the imaginary part ϵ_2 are associated with *interband transitions* (IT) and describe macroscopically the resonant absorption of photons by the medium. The zeros of the real part ϵ_1 (combined with a vanishing ϵ_2) are called volume *plasmon excitation* and correspond to the polarization eigenmodes of the infinite medium. For anisotropic materials, the previous considerations remain valid but imply various combinations of the tensor component.

In finite systems, where boundaries play a large role, surface and interface excitations add their contributions to the bulk excitations. These resonances (modes) are red-shifted compared to bulk-energy modes and directly reflect the geometry of the object: for example, translationally (rotationally) invariant objects have modes indexed by a kinetic (angular) momentum. For isotropic media, this can be illustrated within a simple Drude model for which surface modes arise at $\frac{\omega_p}{\sqrt{2}}$ in the case of a half-space or at

$\sqrt{\frac{l}{2l+1}} \omega_p$ for a filled sphere (l is the angular momentum and ω_p is the plasma frequency of the bulk material). For an object of finite thickness, a slab (or a hollow sphere) for example, such modes split into two branches, one symmetric (tangential) and one antisymmetric (radial), which merge for high thickness of the object or, equivalently, for large momentum transfer [7,8]. The existence of these symmetric and antisymmetric branches was demonstrated experimentally in thin Al foils [5] by electron-energy-loss spectroscopy (EELS) in transmission. The influence of the geometry on the surface-plasmon energy of nanospheres has been shown by spatially resolved EELS in a scanning transmission electron microscope (STEM) [6,9].

In a hollow nanostructure, such as nanotubes or hyperfullerenes, the role of surface is even more pronounced and the understanding of the surface effect on the electromagnetic response of the nanoparticle becomes essential. Moreover, the anisotropy of the nanostructure, which can be local (i.e., the principal crystallographic axis changes rapidly on the scale of the nanostructure), can also greatly affect this surface coupling phenomenon and then the dielectric response of a nanostructure [10–15]. As a matter of fact, when anisotropy is concerned, the connection between the anisotropy, the symmetry, and the energy of the excitations has to be reconsidered. In this Letter, we address these questions by means of an investigation that combines experimental and theoretical approaches to the surface coupling effect in a cylindrical anisotropic material (WS_2 nanotube) in a near-field geometry. WS_2 nanostructures were selected to perform this study because they offer the best versatility in terms of accessible inner and outer diameters, and allow us to distinguish anisotropy and surface coupling effects. WS_2 nanotubes were synthesized according to the procedure described in [16]. Typically, a synthesis yields a large variety of tube diameters, from the thinnest constituted by two or three walls (see a TEM image of a three-wall nanotube in Fig. 1a) to the thickest

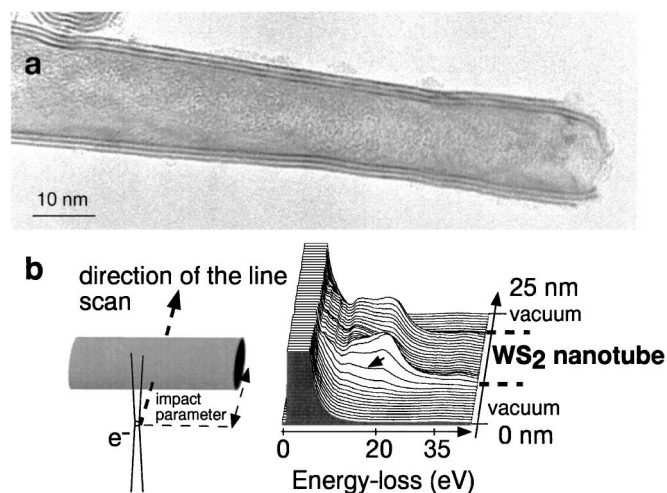


FIG. 1. (a) High-resolution image of a three-wall WS_2 nanotube. (b) A series of spectra acquired while scanning the STEM probe, with corresponding geometry. The arrow indicates the direction of the line scan, which can be accurately determined.

having 20 walls. WS_2 nanotubes are made up of rolled-up WS_2 hexagonal sheets interacting weakly via van der Waals forces. Each sheet is a sandwich of three layers (S-W-S) with covalent tetrahedral W-S bonds. Such structure is locally preserved in the nanotubes, which then are locally anisotropic. The anisotropic axis (c axis) is defined as the axis locally perpendicular to the sheets. In the following, parallel (perpendicular) means parallel (perpendicular) to this axis.

EELS in a STEM is an appropriate tool to investigate such polarizability properties [17–19]. Moreover, its analysis ability at a nanometer scale makes it a perfectly suited technique for the investigation of individual nanoparticles for which strong surface effects are expected. In order to record low-loss EELS spectra (1–50 eV), we have used a STEM in a near-field geometry, where a 0.5-nm probe is positioned at grazing incidence (about 0.5 nm) of a tube (see inset of Fig. 2). The probe position can be monitored with an accuracy better than 0.25 nm. Figure 1b shows a collection of spectra acquired every 3 nm along a line scan across a nanotube of the same dimensions as the one in Fig. 1a. The spectrum acquired at grazing incidence is shown by an arrow. In such geometry only surface modes are excited. The spectra were acquired using a Gatan 666 parallel EELS spectrometer, providing a 0.5-eV resolution with an acquisition time of 0.4 s.

In our previous studies [10] on carbon and boron nitride (BN) nanotubes and nanospheres the coupling effects were not investigated because only thick hollow nanoparticles were fully analyzed. Here, we will show that (1) as for the isotropic and ideal case (i.e., where bulk and thus surface modes are well defined), the surface coupling is revealed by the occurrence of two distinct intensity bands in the EELS spectrum for small wall thickness, with either pure symmetric or antisymmetric character. These bands merge (for thicker wall objects) into a single band. (2) More-

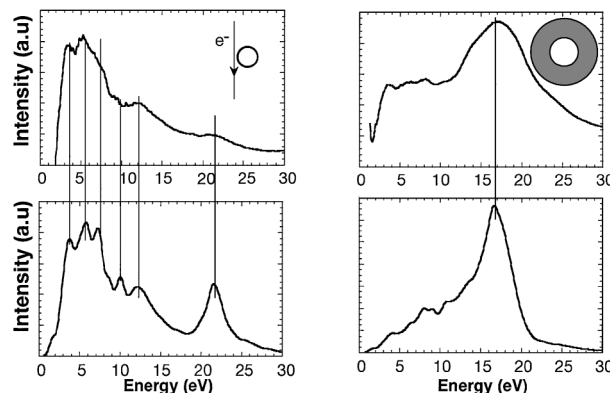


FIG. 2. Experimental (upper curves) and simulated (lower curves) loss spectra for thin (left side) and large (right side) WS_2 nanotubes. Geometry of the experiment and of the tubes are schematically described in the insets.

over, for small shell thickness, the excitation modes of the anisotropic nanoparticles present the following peculiarities: low-energy (symmetric) excitation modes occur at the position of the IT associated with the in-plane component of the dielectric tensor, while the high-energy (antisymmetric) excitation modes occur at the position of the bulk plasmon energy associated with the out-of-plane component.

Experimental data for two extreme situations are shown in Fig. 2. The EELS spectrum from the thinnest tube (Fig. 2a), with external and internal radii $R = 7.4$ nm and $r = 6.0$ nm, respectively, presents a forest of peaks from 0 to 15 eV, and an isolated peak at 22 eV, while that of the thicker nanotube [(see Fig. 2b) $R = 20.5$ nm, $r = 10.5$ nm] shows a broad maximum centered about 16 eV and weaker oscillations at lower energy. Although they mostly differ by the wall thicknesses of the particles, these spectra are strikingly different, and such large variations do not seem to have ever been observed for any type of nanoparticles or thin films.

For the sake of interpreting the data, we have performed EELS simulations by using the dielectric model in the electrostatic limit [7,12,14,20], which proved to be reliable for both isotropic [6] and anisotropic [10] nanoparticles. Briefly, an electron traveling aloof a particle along a classical trajectory excites its surface dielectric modes, which gives rise to an induced field acting back on the electron, producing an energy loss. In [10], we have shown that the main features of the EELS spectra of carbon and BN cylinders can satisfactorily be accounted for, using a simulation for a sphere. As this last geometry is more convenient to deal with, we have therefore performed EELS simulations for WS_2 spheres. The dielectric tensor for bulk planar WS_2 was used for all additional simulations of polarizabilities. It was computed in the optical limit with *ab initio* calculated wave functions using the density functional theory within the local density approximation. Our choice of such a dielectric tensor relies on a satisfactory agreement with experimental values of $\bar{\epsilon}(\omega)$, when available, i.e., for the ϵ_{\perp} case.

The EELS spectrum for a sphere is given by [20] $P(\omega, b) = \sum_l C_l(\omega, b) \text{Im}[\alpha_l(\omega)]$, where l is the angular momentum transfer, C_l is the kinematic factor, b is the impact parameter (i.e., distance from the beam to the center of the particle), and α_l is the response of the particle to a multipolar field of order l . C_l depends on the experimental conditions (impact parameter, acceleration voltage). The polarizability α_l depends uniquely upon the aspect ratio of the particle (inner and outer radii), and on the dielectric tensor of the bulk material [12,14]. Applied to our case, both thin and thick anisotropic shell simulated spectra are shown in Fig. 2, and fit surprisingly well with experimental data despite the lack of similarities between the two cases. This shows that the dissimilarities observed for a specimen of the same nature but different thickness are not due to microscopic phenomena and can be interpreted within the dielectric formalism.

In order to attribute different features of the spectra to specific excitations, we computed the spectra for both the thin and thick tubes, while setting successively either ϵ_{\parallel} or ϵ_{\perp} equal to unity. In such a description, the material cannot be polarized along one (parallel or perpendicular) crystallographic axis. In Fig. 3a, we show that the spectrum of the thin shell tube is the sum of the two contributions. Then, one can directly attribute the high-energy peak to excitations related to ϵ_{\parallel} , and the low-energy features to those of ϵ_{\perp} . On the other hand, such a decomposition fails to describe the thick tube features, as proven by Fig. 3b.

The thickness of the particle seems to be the parameter of importance, much more than the geometry—spherical, cylindrical, or planar. Consequently, we propose to further develop our interpretation by using a simple anisotropic

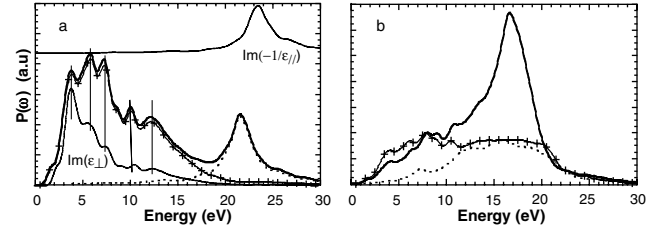


FIG. 3. Calculated spectra for small (a) and thick (b) nanotubes using a dielectric model for spherical particles. Solid lines: calculated spectra using *ab initio* dielectric constant. Dashed lines: same calculations, with $\epsilon_{\perp} = 1$. Cross dots: same calculations with $\epsilon_{\parallel} = 1$. $\text{Im}(\epsilon_{\perp})$ and $\text{Im}(-1/\epsilon_{\parallel})$ are also shown in the left panel.

slab model, which can be analytically worked out much more easily than a curved shell model. Let us assume that we are studying a WS_2 slab of thickness d , with an electron traveling parallel to the slab at an impact parameter b , a situation which will prove to account for the main physics of our experiment. In this case, the c axis of the material is perpendicular to the slab surface. This situation remains locally valid in spherical and cylindrical geometry. The geometrical out-of-plane (in-plane) direction is then equivalent to the anisotropic parallel (perpendicular) direction. The EELS spectrum can then be computed as [21]

$$P(\omega, b) = \int_0^{\infty} dk C_K(\omega, b) \text{Im}[\gamma_K(\omega)],$$

where $K = \sqrt{k^2 + \omega^2/v^2}$ is the modulus of the transferred momentum, k is its component within the plane of the surface, and the response function [the formal equivalent of $\alpha_l(\omega)$ for the planar case] reads [13]

$$\gamma_K(\omega) = - \frac{[1 - \epsilon_{\parallel}(\omega)\epsilon_{\perp}(\omega)] \text{sh}(\frac{Kd}{\sqrt{\lambda}})}{[1 + \sqrt{\epsilon_{\parallel}(\omega)\epsilon_{\perp}(\omega)}]^2 e^{Kd/\sqrt{\lambda}} - [1 - \sqrt{\epsilon_{\parallel}(\omega)\epsilon_{\perp}(\omega)}]^2 e^{-Kd/\sqrt{\lambda}}},$$

where $\lambda = \frac{\epsilon_{\parallel}(\omega)}{\epsilon_{\perp}(\omega)}$ and $C_K(\omega) \propto e^{-Kb}$ is the kinematic factor.

A direct comparison between the slab parameter, Kd , and the sphere parameters l , r , R can be made by means of the relation $[(1 - \frac{r}{R})l = Kd]$ [22]. Knowing that experimentally $l \leq 5$ [10], we derive $Kd \leq 0.5$ for thin tubes ($r/R \approx 0.9$) and $0.5 < Kd < 2.5$ for thick ones ($r/R \approx 0.5$). Let us comment on the two situations: $Kd \ll 1$ (thin tubes) and $Kd \gg 1$ (thick tubes).

For $Kd \gg 1$, the limit of $\gamma_K(\omega)$ gives

$$\gamma_K(\omega) = - \frac{1 - \sqrt{\epsilon_{\parallel}(\omega)\epsilon_{\perp}(\omega)}}{1 + \sqrt{\epsilon_{\parallel}(\omega)\epsilon_{\perp}(\omega)}}$$

which depends only on the geometrical average of the dielectric component, as was already shown for anisotropic half-space [13,23]. For an isotropic material ($\epsilon_{\perp} = \epsilon_{\parallel} = \epsilon$), one retrieves the standard surface dielectric response $\gamma_K(\omega) = -\frac{1-\epsilon}{1+\epsilon}$ [18]. If the resonances of the parallel and perpendicular dielectric components overlap in energy, as is the case for WS_2 , there is no possibility to discriminate between excitations related to an in-plane or out-of-plane

component of the dielectric tensor. This explains why the decomposition of the spectrum for a thick tube in Fig. 3b does not work.

In the limit $Kd \ll 1$, we find $\gamma_K(\omega) = \frac{Kd}{4} [\frac{-1}{\epsilon_{\parallel}(\omega)} + \epsilon_{\perp}(\omega)]$, which is clearly disymmetric with respect to the \perp and \parallel components. Resonances of $\text{Im}[\gamma_K(\omega)]$, and then of $P(\omega)$, occur at maxima of $\text{Im}[\epsilon_{\perp}(\omega)]$ and $\text{Im}[-\frac{1}{\epsilon_{\parallel}(\omega)}]$. In Fig. 3a we compare the calculation of the two terms of the analytical expression in the small Kd limit to the full simulation for a WS_2 nanosphere. Considering that (i) the above expression has been obtained for an anisotropic slab and (ii) the small Kd limit is not fully reached, we clearly evidence two bunches of modes, associated with resonances of $\text{Im}[\epsilon_{\perp}(\omega)]$ and $\text{Im}[-\frac{1}{\epsilon_{\parallel}(\omega)}]$, which merge in the case of thick tubes.

For ideal isotropic thin films, the surface coupling is responsible for two branches of modes which are associated with the symmetric and antisymmetric behavior of the electric potential. As emphasized by the induced potential maps of Fig. 4, this association can be generalized to a real

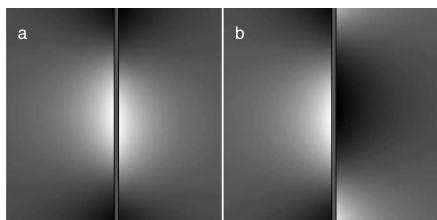


FIG. 4. (a),(b) Maps of the induced potential of a WS_2 slab for energies 7.8 and 23 eV. The maps are computed using an *ab initio* dielectric constant and the electrostatic dielectric model, with no other fitting or approximation. Note the symmetric (antisymmetric) behavior of the low-energy (high-energy) excitation.

and anisotropic thin material. Indeed, the induced potential associated with any of the low energy modes [for instance, 7.8 eV (Fig. 4a)] and the one associated with the high-energy modes [for example, 23 eV Fig. 4b)] display, respectively, symmetric and antisymmetric behavior. Moreover, the link between the anisotropy and the symmetry is clearly revealed, since we can associate the symmetric mode to a maximum of $\text{Im}[-\frac{1}{\epsilon_{\parallel}}(\omega)]$ (Fig. 4a) and the antisymmetric mode to a maximum of $\text{Im}[\epsilon_{\perp}(\omega)]$ (Fig. 4b). Further calculations show that a complete analogy to the case of a slab can be made for an anisotropic shell: the tangential mode and the radial modes (as defined in the isotropic case [8]) are the counterparts of the symmetric and antisymmetric modes. This description is very similar to that for phonon excitation modes, where, for small thickness, modes decouple into longitudinal and transverse optical phonons [24].

In conclusion, the puzzle of the effect of surface coupling in anisotropic media has been solved by studying the surface modes of WS_2 nanostructures with different geometries, using spatially resolved EELS. Beyond the isotropic case, we have shown that the surface coupling in an anisotropic nano-object results in the existence of symmetric (tangential) and antisymmetric (radial) modes, even in real solids. Moreover, we reconsidered the definition of *surface-plasmon* resonances, as they arise at the *bulk-plasmon* resonance of the *parallel* dielectric constant, and at the *interband transition* of the *perpendicular* component of the dielectric tensor. The classical model is quite successful in interpreting our data even when the layers are a few atoms thick, similar to the case encountered when describing optical properties of small clusters with dielectric theories [25].

We acknowledge E. Sandré for providing us with the *ab initio* calculations, and Ph. Lambin and A. A. Lucas for fruitful discussions. L.H. was supported by the Belgian National Fund (FNRS). This work was partly funded by

the Belgian Interuniversity Research Project on Reduced Dimensionality Systems (PAI-UAP P4-10).

-
- [1] T. W. Ebbesen, H. J. Lezec, H. F. Ghaemi, T. Thio, and P. A. Wolff, *Nature (London)* **391**, 667 (1998).
 - [2] T. Klar, M. Perner, S. Grosse, G. von Plessen, W. Spirkl, and J. Feldmann, *Phys. Rev. Lett.* **80**, 4249 (1998).
 - [3] N. Nilius, N. Ernst, and H. J. Freund, *Phys. Rev. Lett.* **84**, 3994 (2000).
 - [4] J. R. Krenn, A. Dereux, J. C. Weeber, E. Bourillot, Y. Lacroute, J. P. Goudonnet, G. Schider, W. Gotschy, A. Leitner, F. R. Aussenegg, and C. Girard, *Phys. Rev. Lett.* **82**, 2590 (1999).
 - [5] R. B. Pettit, J. Silcox, and R. Vincent, *Phys. Rev. B* **11**, 3116 (1975).
 - [6] D. Ugarte, C. Colliex, and P. Trebbia, *Phys. Rev. B* **46**, 1794 (1992).
 - [7] H. Raether, *Surface Plasmon*, Springer Tracts in Modern Physics Vol. 3 (Springer-Verlag, Berlin, 1988).
 - [8] Ph. Lambin, A. A. Lucas, and J. P. Vigneron, *Phys. Rev. B* **46**, 1794 (1992).
 - [9] M. Achéche, C. Colliex, H. Kohl, A. Nourtier, and P. Trebbia, *Ultramicroscopy* **20**, 99 (1986).
 - [10] M. Kociak, L. Henrard, O. Stéphan, K. Suenaga, and C. Colliex, *Phys. Rev. B* **61**, 13 936 (2000).
 - [11] T. Stöckli, J. M. Bonard, A. Châtelain, Z. L. Wang, and P. Stadelmann, *Phys. Rev. B* **61**, 5751 (2000).
 - [12] A. A. Lucas, L. Henrard, and Ph. Lambin, *Phys. Rev. B* **49**, 2888 (1994).
 - [13] Ph. Lambin, P. Senet, A. Castiaux, and L. Philippe, *J. Phys. I (France)* **3**, 1417 (1993).
 - [14] L. Henrard and Ph. Lambin, *J. Phys. B* **29**, 5127 (1996).
 - [15] C. Yannouleas, E. N. Bogachek, and U. Landman, *Phys. Rev. B* **50**, 7977 (1994).
 - [16] R. Tenne, L. Margulis, M. Genut, and G. Hodes, *Nature (London)* **360**, 444 (1992).
 - [17] R. H. Ritchie, *Phys. Rev.* **106**, 874 (1956).
 - [18] Z. L. Wang, *Micron* **27**, 265 (1996).
 - [19] H. Cohen *et al.*, *Phys. Rev. Lett.* **80**, 782 (1998).
 - [20] T. L. Ferrell and P. M. Echenique, *Phys. Rev. Lett.* **55**, 1526 (1985); P. M. Echenique, A. Howie, and D. J. Weathley, *Philos. Mag. B* **56**, 335 (1987).
 - [21] P. E. Batson, *Ultramicroscopy* **11**, 299 (1983); A. Howie and R. H. Milne, *Ultramicroscopy* **18**, 427 (1985).
 - [22] L. Henrard, O. Stéphan, and C. Colliex, *Synth. Met.* **103**, 2502 (1999).
 - [23] A. A. Lucas and J. P. Vigneron, *Solid State Commun.* **49**, 327 (1984).
 - [24] K. L. Kliewer and R. Fuchs, *Adv. Chem. Phys.* **XXVII**, 355 (1974).
 - [25] C. Bréchnignac, Ph. Cahuzac, and N. Kébaïli, J. Leygnier, and H. Yoshida, *Phys. Rev. B* **61**, 7280 (2000).